



Synthesis of Er doped ZnO cone-like nanostructures with enhanced structural, optical and magnetic properties

Dhirendra Kumar Sharma^{1,2} · Kapil Kumar Sharma¹ · Vipin Kumar¹ · Anuradha Sharma²

Received: 28 September 2017 / Accepted: 23 November 2017 / Published online: 28 November 2017
© Springer Science+Business Media, LLC, part of Springer Nature 2017

Abstract

In this report, undoped ZnO and Er doped ZnO nanostructures [$\text{Zn}_{1-x}\text{Er}_x\text{O}$, where $x = 1, 3, 5$ and 7 at. %] were synthesized by chemical precipitation technique. The chemical precipitation route for the preparation of undoped ZnO and Er doped ZnO nanostructures at different concentrations represents an easy, fast and efficient method. The synthesized nanostructures were characterized to analyze their crystal structure, crystal morphology, optical and magnetic properties using X-ray diffraction (XRD), Energy dispersive X-ray (EDX), High resolution scanning electron microscopy (HRSEM), Ultraviolet–Visible spectroscopy (UV–Visible), Photoluminescence spectroscopy (PL) and Vibrating sample magnetometer (VSM) respectively. The XRD studies exposed that undoped ZnO and all Er doped ZnO samples have a hexagonal wurtzite crystal structure. The XRD results showed that Er^{3+} ions were successfully doped into ZnO nanostructures as no diffraction peaks of Er or erbium oxide were observed in the pattern. EDX results also confirmed that Er ions were successfully incorporated into the lattice position of Zn ions in ZnO. HRSEM characterization showed that presence of Er^{3+} ions in crystal structure of ZnO can change the morphology i.e. the transformation of nanorods to nanocones. Nanorods-like structure obtained with 1 at. % Er extend to nanocones-like for 3–7 at. % Er doped ZnO with changes in length and thickness in nm range. In UV–Visible absorbance spectra, a red shift was observed in the band gap of undoped ZnO and Er doped nanostructures with increasing Er concentration. PL measurements also revealed that the undoped ZnO and Er doped ZnO nanostructures had an UV emission, a defect emission and the Er ions doping induced a red shift in the UV emission with a small enhancement in the defect emission. The VSM study revealed that the undoped ZnO and Er doped ZnO nanostructures exhibit paramagnetic and ferromagnetic behaviour at room temperature respectively.

1 Introduction

In recent years, great deals of research efforts have been done on developing uniquely versatile metal oxide nanomaterials with superior properties which are not observed in conventional materials in technological applications. Zinc oxide (ZnO) is one of the most comprehensively studied materials in this category of II–VI semiconductors due to its high direct band gap ~ 3.4 eV, large exciton binding energy (60 meV) and a large conducting range from 10^4 – 10^{-12} ohm cm. In optoelectronic devices, ultraviolet lasers, gas sensors, solar cell, photo catalyst and light

emitting diodes; ZnO is the most widely used due to its direct wide band gap energy, high electron mobility and luminescence etc. [1–5]. This oxide is economical, environment friendly having high sensibility, low cost and revealing a high thermal and chemical stability, which makes it even more usable and acceptable [6, 7]. In the present times, the greatest concern of researchers is to remove hazardous pollutants from air and water and ZnO has reflected better photocatalytic efficiencies in comparison to TiO_2 , which can remove organic compounds in water matrices based on its larger initial activity rates and its efficient absorption of solar radiation [8, 9].

The crystal structure, morphology, size and surface defects are the important characteristics on which the properties of ZnO nanostructures depend. It's been proved that alteration of ZnO nanostructures could enrich their properties through doping of transition metals or rare earth (RE) elements [10–14]. If RE elements integrated into suitable matrices; which is an emerging topic of eminence for their

✉ Dhirendra Kumar Sharma
dhirajvasistha@gmail.com

¹ Department of Physics, KIET Group of Institutions, Ghaziabad, India

² Department of Physics, YMCA University of Science and Technology, Faridabad, India

partially filled $4f$ shells surrounded by completely filled $5s$ and $5p$ shells, their intra $4f \rightarrow 4f$ optical transitions become possible [15]. The modification with the incorporation of dopant ions significantly enhanced the photocatalytic and sensing performance of ZnO [16, 17]. Undoped ZnO exhibits the paramagnetic behaviour whereas the transition or RE element doped ZnO has been detected to exhibit ferromagnetic characteristic at room temperature [18–22]. The extensive studies about RE elements doped ZnO is conducted for industrial application in the field of spintronic, photoluminescence, laser, fibre amplifier and so on [23–27]. Erbium (Er), out of the various RE elements, is an important focus of attention because of its enormous potential in various applications. Although ZnO is a good matrix material to host the Er ions as it is not only responsible for the allowance of $4f$ transition, prohibited in isolated atom but also for the reason that it enhances the emission yield for the transition [28, 29].

Considering the above as base, this work explores the fact that using a simple chemical precipitation technique undoped ZnO and a series of Er doped ZnO samples were prepared. Until now, RE doped ZnO nanostructures have been synthesized by different method such as pulsed laser deposition, magnetron synthesis, chemical vapour deposition, spray pyrolysis, solution combustion and vapour transport route [30–33]. An important role is played by the synthesis method in enhancing the properties of materials. The production of huge amounts of high uncontaminated samples at low cost is facilitated by the conventional chemical precipitation method. Present work exposes and diminishes the controversies that still exist regarding whether RE elements could be incorporated into the semiconductor nanocrystals or not, and if; whether efficient energy transfer from the ZnO host to RE element could occur or not. This work exhibits that doping of Er ion can be effectively done in ZnO nanostructures with some parameters of chemical precipitation method such as solution properties, mixing rate, pH value and drying treatment. The prepared samples were characterized by XRD, HRSEM, EDX, UV/Visible spectroscopy, PL and VSM. The improved structural transformation, luminescence, ferromagnetism characteristics and a decrease in band gap energy has been reported in this paper. It's low cost, high yield and ability to attain high purity in fabrication of undoped ZnO and Er doped ZnO nanostructures proved chemical precipitation to be highly advantageous method.

2 Experimental details

In the present investigation, Er doped ZnO and the undoped ZnO powders were prepared via the chemical precipitation route. All the reagents used were of analytical grade (Sigma-Aldrich) without further purification. Er doped ZnO powders were prepared by zinc acetate

[$\text{Zn}(\text{CH}_3\text{COO})_2 \cdot 2\text{H}_2\text{O}$; 99.5% purity], Erbium(III) oxide [Er_2O_3 ; 99.9% purity], sodium hydroxide [NaOH; 98% purity] and ammonium hydroxide [NH_4OH ; 99.99% purity]. Four batches of samples were prepared by varying the different molar concentration of doping erbium oxide in zinc acetate as 1, 3, 5 and 7 at.%. As per described Er doping concentration, the calculated amount of erbium oxide solution was added to zinc acetate solution. In this foundation solution, 1 M solution of ammonium hydroxide and sodium hydroxide was added drop-wise. The ammonium hydroxide and sodium hydroxide were used as OH^- source for forming the complexes and to control the pH value of solution respectively. During the entire process, magnetic stirring was carried out to achieve the precipitate of Er doped ZnO samples. Undoped ZnO powder was formed by zinc acetate, sodium hydroxide and ammonium hydroxide. Zinc acetate and ammonium hydroxide were dissolved into de-ionized (DI) water with magnetic stirring until they form clear solutions. Sodium hydroxide (1M) solution was added drop-wise into the prepared clear solution of zinc acetate and ammonium hydroxide with constant magnetic stirring. In both cases, these precipitates were thoroughly washed several times with DI water to remove the unwanted ions. These washed precipitates were dried at 60°C for 2 h. These dried precipitates were grinded and added 100 ml DI water and again dried at 60°C for 40 h followed by normal cooling up to the room temperature; then final powder products were collected carefully. As per the established literature on chemical precipitation technique leading to the formation and controlling of undoped ZnO and Er doped ZnO nanostructures is critical. Due to this reason, the slow mixing of reactants and the pH value (~ 12) of all samples were kept constant during synthesis process.

The crystalline phase and structural information of prepared samples were studied by using a Bruker D8 Advance X-ray diffractometer with $\text{CuK}\alpha$ radiation of wavelength $\lambda = 0.15405$ nm. All XRD measurements were performed in the range of $2\theta = 20^\circ\text{--}90^\circ$ at a scan speed of $3^\circ/\text{min}$ at room temperature. Surface morphology and chemical composition of samples were investigated by using a JEOL JEM-2100F HRSEM equipped with EDAX equipment. The nanostructures were also analyzed by dissolving Er doped ZnO nanostructures in DI water followed by ultrabath sonication for 20 min. The samples were subjected to optical characterizations. The UV–Visible spectra of prepared samples were carried out by using JASCO UV–Visible spectrophotometer (Model-Lambda). PL measurements of prepared samples were made by employing Lab RAM UV–Vis–NIR spectrometer Horiba Yvon having The-Cd 325 nm. Magnetic properties of the synthesized samples were obtained from VSM at room temperature.

3 Results and characterization

3.1 XRD characterization

The XRD patterns of undoped ZnO and Er doped nanostructures [Zn_{1-x}Er_xO, where x = 1, 3, 5 and 7 at.%] have been analysed about crystallographic and structural information. Powder XRD patterns of undoped ZnO and Er doped ZnO samples are plotted against intensity versus 2θ in range of 30°–75° in the Fig. 1i. All the patterns are in close agreement with the standard XRD data (JCPDS file no. 36-1451) indicating the hexagonal wurtzite structure. The prominent diffraction peaks observed at 31.79°, 34.52°, 36.24°, 47.60°, 56.58°, 62.95°, 68.04°, and 69.12° respond from lattice planes (100), (002), (101), (102), (110), (103), (112) and (201) respectively. This graph shows that Er³⁺ ions sit at the host Zn²⁺ sites without disturbing the wurtzite structure because no extra peaks obtained from Er related second phase than those of ZnO such as Er₂O₃. The peaks in the diffraction pattern of Er doped samples show slightly shifting towards lower angles as compared to undoped ZnO.

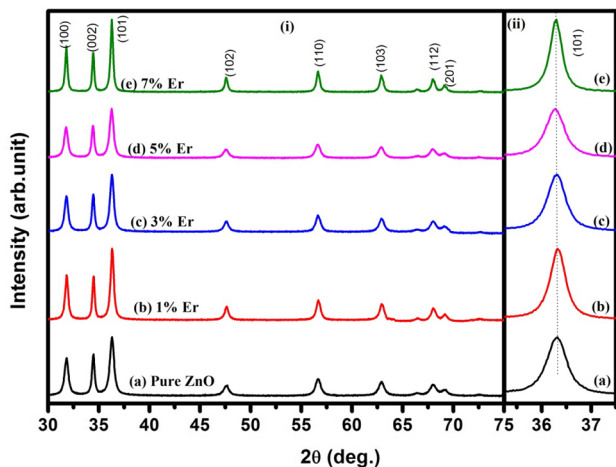


Fig. 1 i XRD pattern of a undoped ZnO, b 1, c 3, d 5, and e 7 at.% Er doped ZnO nanostructures, ii shifting of (101) peak for respective nanostructures

Table 1 Average crystallite size, lattice constants, bond length and cell volume of undoped ZnO and Er doped ZnO samples

Concentration of Er (%)	Average crystallite size D (nm)	Lattice constant c (Å)	Lattice constants a=b (Å)	Bond length of anion–cation L (nm)	Cell volume V (Å ³)
0	15.99	5.2817	3.2344	1.9806	47.8846
1	17.03	5.2866	3.2374	1.9825	48.0196
3	17.57	5.2824	3.2348	1.9809	47.9022
5	21.10	5.2786	3.2324	1.9794	47.7959
7	27.84	5.2836	3.2355	1.9813	47.9357

The trend of (101) peak shifting with different Er doping as shown in Fig. 1ii, is of particular interest here. This means that the lattice parameter increases with the Er doping which is an expected result because the ionic radius of Er³⁺ (0.88 Å) is greater than the ionic radius of Zn²⁺ (0.74 Å). The average crystallite size of samples has been calculated, using the Debye Scherrer's formula:

$$D = \frac{0.9\lambda}{\beta \cos \theta}$$

where λ is wavelength of the CuKα radiation (0.15405 nm), β and θ are the FWHM and the diffraction angle of the observed peaks using the diffraction intensity of (101) lattice plane. In order to examine the doping effect of Er concentration on the crystal parameters of prepared nanostructures, the lattice parameters, bond length and volume of unit cell for hexagonal system have been calculated using lattice geometry equation.

$$\frac{1}{d^2} = \frac{4}{3} \left(\frac{h^2 + hk + k^2}{a^2} \right) + \frac{l^2}{c^2}$$

where d is the inter-planer spacing between the planes and h, k and l are miller indices. The bond length (Zn–O) can be calculated using this formula,

$$l = \sqrt{\frac{a^2}{3} + (0.5 - u^2)c^2}$$

where a and c are lattice constants of ZnO and u is the wurtzite structure parameter which can be calculated as,

$$u = \left(\frac{a^2}{3c^2} \right) + \frac{1}{4}$$

In addition, the volume of unit cell has been calculated using the formula,

$$V = 0.866a^2c$$

All these parameters of samples are summarized in Table 1. From the Table 1, no fixed pattern of variation in the calculated crystal parameters could be observed for these nanostructures on comparing previously reported literature [34–36]. Only a fixed increasing pattern in D (crystallite

size) is observed from 0 to 7 at.% Er doped ZnO. But as the doping concentration increases, the slight variation in lattice constants, bond length and volume of unit cell could be due to Zn and Er ionic size mismatch and the replacement of Zn^{2+} ions with the Er^{3+} ions in the crystal lattice.

3.2 EDX characterization

In order to confirm the presence of Er^{3+} ion and determine its chemical composition, EDX analysis of 1 and 5 at.% Er doped samples were carried out. The EDX of 1 and 5 at.% Er doped samples is shown in Fig. 2a, b. For accuracy, EDX measurement was carried out at a number of locations all over the sample. From EDX analysis the presence of Zn, Er and O elements were confirmed in the sample. According to the EDX analysis Zn and Er contents in the composition of 1 and 5 at.% Er doped samples are close to the proposed doping concentration. All the above results of XRD and EDX indicate that the Er^{3+} ions are

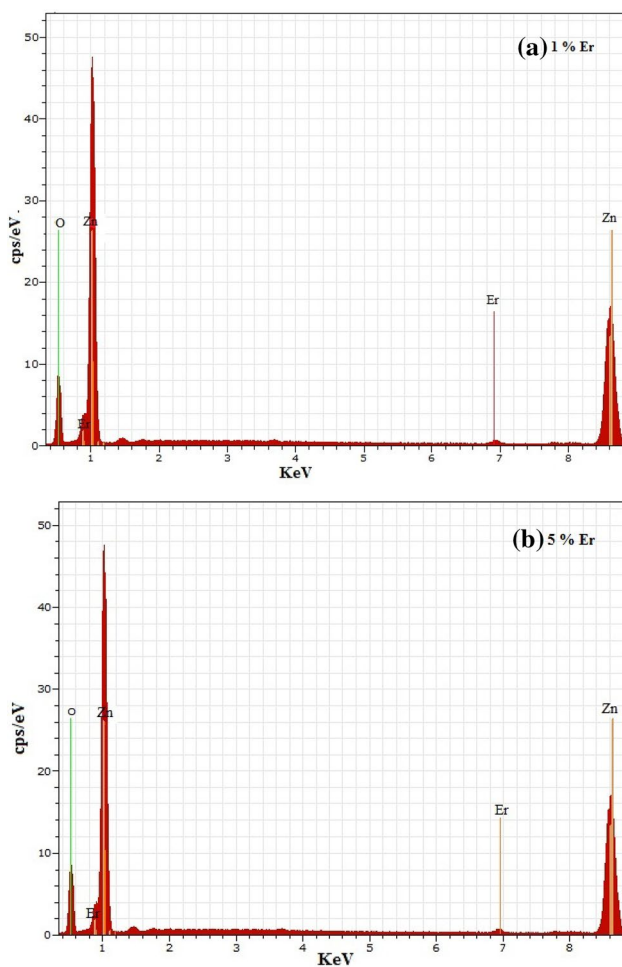


Fig. 2 EDX spectrum of **a** 1 and **b** 5 at.% Er doped ZnO nanostructures

effectively doped into the crystal lattice of ZnO matrix without forming erbium oxides or any other impurities at the surface of ZnO.

3.3 HRSEM characterization

The morphological features of prepared samples were carried out by using HRSEM images. The incorporation of Er ion in Zn lattice sites makes the changes in the morphology of crystallites. Figure 3a–e shows HRSEM images of undoped ZnO and Er doped ZnO samples, where structures are in the nm range. The distribution of sizes as well as shape is irregular and this may be due to the damages occurred in the re-crystallisation or coalescence of nanostructures in formation of larger agglomeration of ZnO lattice during the heating process. As shown in Fig. 3a, the surface texture of undoped ZnO is irregular in shape and is found to be in 50 nm range.

It is observed that the doping of Er with ZnO remarkably changed the morphology of the nanostructures from nanorods-like to nanocones-like, as shown in Fig. 3b–e. For 1 at.% Er doped ZnO nanorods of approximately 100 nm long and 25 nm thick are observed in Fig. 3b, which is similar to undoped ZnO nanostructures, influence of Er doping on size or shape is not observed at this stage. For 3 at.% Er doped ZnO nanorods of approximately 200 nm long and 50 nm thick are seen in Fig. 3c. Infact onset of structural transformation is evident for 3 at.% Er. At this stage, enhanced Er doping induced anisotropic growth not only causes the formation of nanorods but here onwards, the evolution of nanocones initiates as marked through the dashed lines in Fig. 3c. The systematic transformation continues with further Er doping and is vividly evident for 5 and 7 at.% Er doped nanostructures, as shown respectively through Fig. 3d, e. The dominant growth of structure for 7 at.% Er doping is demonstrated clearly through the formation of approximately 400 nm long and 70 nm thick structure of nanocones-like as exhibited in Fig. 3e.

Therefore the observed changes in structures can only be attributed to the effects of dopant, which might act as structure driving agents through selectively adsorbing onto ZnO crystalline planes. Structurally ZnO has three types of crystalline planes—two non-polar (2110) and (0110) planes and a polar (0001) basal plane. The polar basal plane has high surface energy as compared to non-polar planes [37]. Furthermore, under thermodynamic equilibrium condition the facets with higher surface energy are usually smaller in surface area whereas the lower energy facets are larger [38]. Therefore the growth of crystals in c axis direction is faster which leads to the formation of nanorod to nanocone shape crystal as it is indicated in Fig. 3b–e.

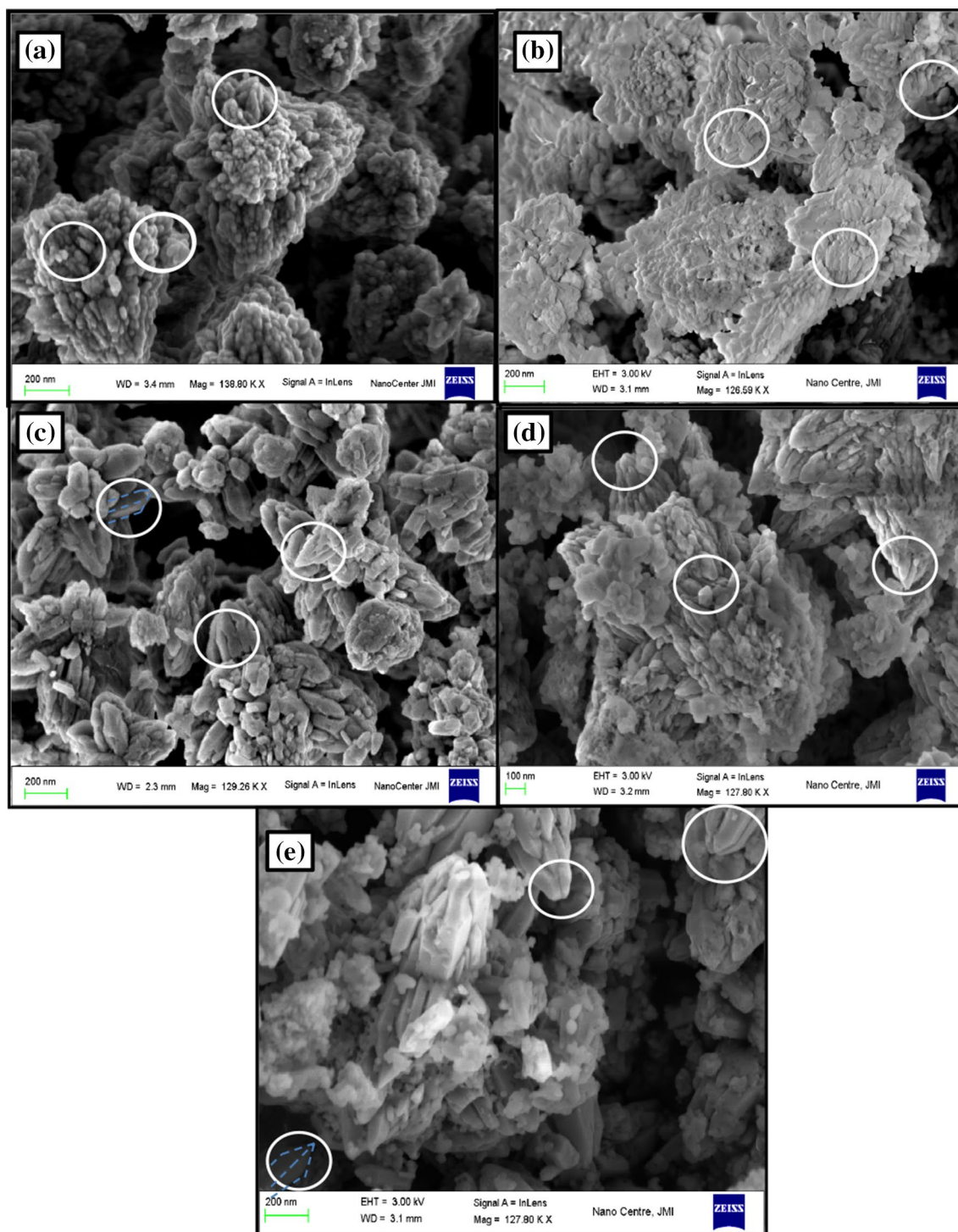


Fig. 3 HRSEM images of **a** undoped ZnO, **b** 1, **c** 3, **d** 5, and **e** 7 at.% Er doped ZnO nanostructures

3.4 UV-Visible characterization

As doping is an effective way to alter the optical and electrical properties of semiconductor materials. To further improve the performance of their optoelectronic devices, RE

elements have always attracted a large group of researchers [39–49]. RE elements such as Eu, Tb, Yb, and Nd are the famous visible luminescence centers once they are incorporated into the host matrix [39–41]. Therefore, it is widely expected that doping of RE element into the ZnO lattices

would open the channels for efficient visible light emissions [39]. Recently, Eu^{3+} ion as one of the most famous red emitting activators has been successfully incorporated into the ZnO nanoparticles, nanorods arrays, and nanospheres and most of them provide the red emission at 615 nm due to the intra $4f$ shell $5D_0 \rightarrow 7F_2$ transitions, which makes Eu doped ZnO a promising candidate for the white light-emitting diode and planar display due to their multi-colour emissions [39]. However, there are few reports for Er^{3+} ion doped ZnO nanoparticles [30, 42]. The interest of Er doping originates from the motivation to doping the dissimilar element (here in our case Er) in ZnO lattice due to the huge differences in their ionic radii ($\text{Er}^{3+} = 0.88 \text{ \AA}$) and charges between Zn^{2+} and Er^{3+} ions [39]. Thus, based on previous data, it is crucial to detect the changes observed due to Er doping in electronic levels by recording the absorption spectra of UV–Visible spectroscopy of the prepared nanostructures (as shown in Fig. 4).

As shown in Fig. 4a, one can observe a small hump at 3.34 eV (371 nm) for undoped ZnO nanostructures. This shows that the prepared nanostructures are depicting a slight blue shift as compared to bulk ZnO materials ($\text{Bulk}_{\text{ZnO}} = 3.2 \text{ eV}$) [10]. On doping the 1 at.% Er in ZnO (Fig. 1b), the band gap shows a slight red shift from 3.34 to 3.3 eV (375 nm). This trend of red shift in band gap continuously observed at 3.26 eV (380 nm), 3.20 eV (387.5 nm), and 3.19 eV (388.7 nm) for 3, 5 and 7 at.% doping concentration of Er^{3+} ion in ZnO nanostructures (Fig. 4b–e) respectively. Our results are in good agreements with the previously published report [30]. Another observation which can be derived from Fig. 4 is the corresponding area and peak intensity increase with increasing the doping concentration from 1 to 7 at.% Er in ZnO host lattice. This peak

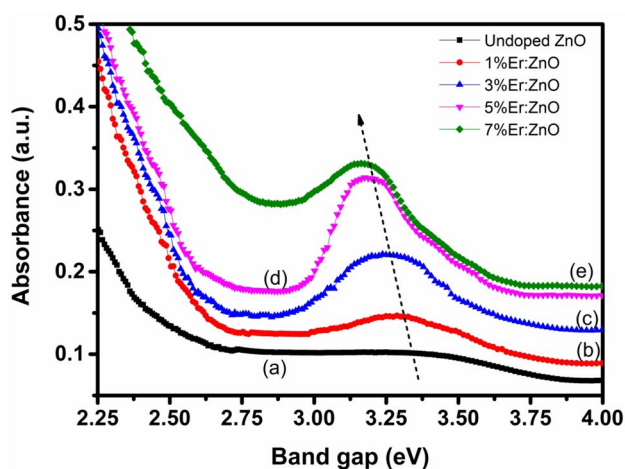


Fig. 4 Room temperature UV–Visible spectra of *a* undoped ZnO, *b* 1, *c* 3, *d* 5, and *e* 7 at.% Er doped ZnO nanostructures. The red shift in band gap is depicted by the line with dotted arrow with increasing Er doping. (Color figure online)

broadening and red shift in band gap signifies the incorporation of Er in ZnO nanostructures [30]. This red shift in band gap prompted us to further perform the luminescence study as is discussed ahead.

3.5 PL characterization

Optical properties of ZnO nanostructures become increasingly important as the size of structures is reduced to nanoscale [43]. The parameter related to surface and size confinement effects of nanomaterials not only vary the band gap but also influence their optical transitions, such as luminescence [10]. Generally ZnO exhibits a visible deep level emission with a peak in the range from 450 to 730 nm [44]. Among the various luminescence properties of ZnO nanoparticles, the green emission around 521 nm is usually reported [43]. Another way to alter the luminescence centres in ZnO is to dope it with either transition elements or with RE elements like Eu, Er [39]. Previously, Eu doping in ZnO lattice pointed out that the host lattice transfer the energy resonantly to Eu^{3+} ion by trapping as oxygen vacancy and energy storage centers [39]. Furthermore, doping of RE elements helps in revealing the fundamental phenomenon of nano-order surface effects by utilizing the PL technique, since it is an effective method to gain a good understanding and systematically investigate the luminescence mechanism and the excitation pathways of the RE^{3+} ions in semiconductor hosts [39]. Therefore, we present the PL emission spectra of Er doped ZnO nanostructures as shown in Fig. 5. In Fig. 5, we have labelled the four peaks based on their intensities from peak 1–4 and elaborate their discussions in the order of decreasing intensities.

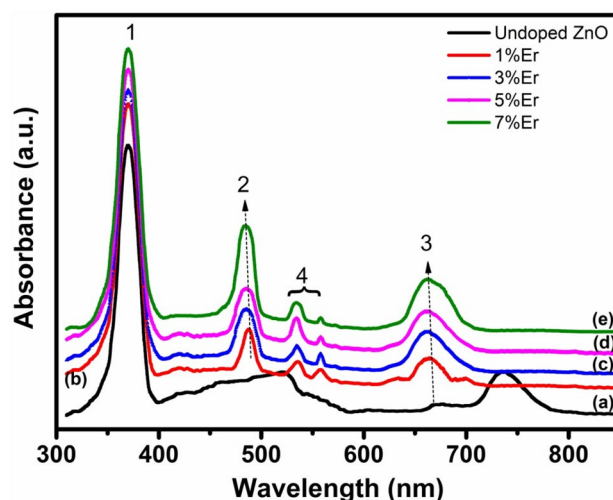


Fig. 5 Room temperature Photoluminescence emission spectra of *a* undoped ZnO, *b* 1, *c* 3, *d* 5, and *e* 7 at.% Er doped ZnO nanostructures

First, we define the transitions occurring in undoped ZnO nanostructures shown by Fig. 5a. Peak '1' corresponds to the band energy transitions occurring at 371 nm thus depicting the quantum confinement effect of nanosize occurring therein [10]. A huge hump ranging from 400 to 600 nm centred at 521 nm is the widely reported for green emission. Although a variety of literature is reported for this emission but this peak in undoped ZnO nanostructures is corresponding to the radiative recombination of the photo-generated hole with an electron occupying the oxygen vacancy [43, 45]. As previously reported that for wurtzite structure of ZnO, valence band (VB) lies in O-2*p* state while Zn have a 4*s*-O 2*p* σ^* interaction which is mainly responsible for two lowest conduction band (CB) that covers a bandwidth of -10 eV. There is dispersion in the VB due to different factors out of which one major reason is overlapping of filled Zn 3*d* and O 2*p* orbitals [46]. Since ZnO is an n-type semiconductor, most defects are Zn interstitials (I_{Zn}) and oxygen vacancies (V_O) [10]. It is well known that visible luminescence is mainly due to defects that are related to deep level emissions such as I_{Zn} and V_O [43]. Visible luminescence in ZnO is primarily caused by the transition from deep donor level to VB due to oxygen vacancies and by the transition from CB to deep acceptor level due to impurities and defect states [43]. The structure of nanosize ZnO contains large voids, which can easily contain interstitial atoms and thus the appearance of blue emission in prepared ZnO nanostructures appear as a huge hump originating from 400 to 600 nm depicting the formation of interstitial defects of Zn [47]. ZnO has tightly bound 2*p* electrons of oxygen and 3*d* electrons of Zn, which have some attraction affinity [43]. Also, previous first principal calculations concluded that the Zn 3*d* electrons interact strongly with the 2*p* electron of O in ZnO structure [48]. As the centre energy of the green peak is different from the band gap energy of bulk ZnO (3.2 eV), this emission cannot be a result of direct recombination of a conduction electron in the Zn 3*d* band and a hole in the O 2*p* VB. Therefore, green emission must be related to the local level in band gap [43]. In fact the green emission results from the radiative recombination of photo generated hole with an electron occupying the oxygen vacancy [45]. We now explain the peak observed for orange-red emission around 736 nm corresponds to defects such as V_O [49].

Having explained the origin of green and orange-red emissions in undoped ZnO nanostructures, we now explain the changes observed in luminescence properties with Er doping in ZnO lattice. It has been previously reported that among the different RE ions, Er occupies a relevant position because of its crucial functioning in the up conversion phenomena and the intense 0.8 eV intra-ionic emission usually referred to as the 1.54 μ m has a very special importance for the optical communications [30]. On the other hand, ZnO is a good matrix material to host the

Er ions since not only is it responsible for 4*f* transitions, which were prohibited in isolated atoms, but also because it improves considerably the emission yield for these transitions [30]. Previously in a report, lower dopant concentration leads to a noticeable quantity of nanostructures but also resulted in poor luminescent properties while higher Er concentrations give rise to very irregular and disordered structures [30]. The reason behind this was the probable stresses induced by the large Er ions in the ZnO structure [30]. Also, low doping concentration < 3 at.% detection limit of XRD is difficult to be examined, as in our case no extra impurity or precursor phase was observed in XRD. But the luminescence characterizations bring out the probable transitions occurring therein. The results are discussed ahead.

As seen in Fig. 5a–e, the most prominent peaks are labelled as peak '1'. These peaks are observed at 371, 375, 380, 387, and 388 nm for undoped ZnO, 1, 3, 5 and 7 at.% Er doped ZnO nanostructures respectively. These most intense transitions observed in prepared nanostructures correspond to inter band transitions from VB to CB [30]. However, one can notice a slight red shift in the wavelength depicting the similar behaviour observed through UV–Visible spectroscopy. Therefore, these peaks are in excellent agreement with UV–Visible analysis thus endorsing our results. One can observe the second and third intense peaks, labelled as '2' and '3', respectively in Fig. 5a–e. These peaks represent the blue and yellowish-red band transitions occurring due to Er doping in ZnO lattice. The intensity of the emission of peak '2' at 488 nm (2.54 eV) increases with increase in Er doping in ZnO nanostructures. This blue emission at 488 nm has been reported for the transfer of energy between Er^{3+} excited ions present in the system and corresponds to ${}^4F_{7/2} \rightarrow {}^4I_{15/2}$ Er transitions [30]. On the other hand, the peak '3' at 652 nm (1.90 eV) emission is the third intense peak. This band is usually attributed to the oxygen excess taking into account the usage of doping with erbium oxide, is consistent with a major incorporation of oxygen present in dopant ZnO nanostructures [30]. This is also in good agreement with the absence of red band at 736 nm peaks, earlier present in Fig. 5a for undoped ZnO nanostructures, for oxygen vacancy in ZnO nanostructures. Lastly, peaks at 558.6 nm (2.22 eV) and 536.8 nm (2.31 eV), corresponding to ${}^4S_{3/2} \rightarrow {}^4I_{15/2}$ and ${}^2H_{11/2} \rightarrow {}^4I_{15/2}$ transitions, respectively have much lower intensity as compared to other marked peaks. The relative intensities of these emissions are also a probe of the defect structure and quality of the nanostructures, since it is earlier reported that the transitions and their intensities are sensitive to local configuration of the particular ion involved in the transition and as a result their intensities diminish [30].

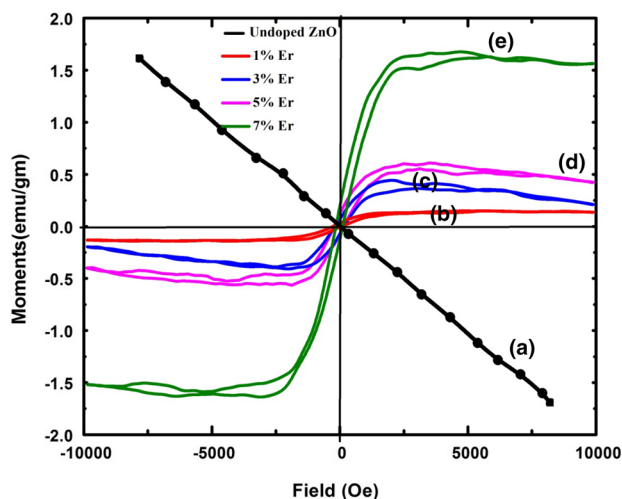


Fig. 6 M–H curve for *a* undoped ZnO, *b* 1, *c* 3, *d* 5, and *e* 7 at.% Er doped ZnO nanostructures

3.6 Magnetic characterization

To further understand the alternation in magnetic properties of undoped ZnO and Er doped ZnO nanostructures [$\text{Zn}_{1-x}\text{Er}_x\text{O}$, where $x = 1, 3, 5$ and 7 at.%] systematic room temperature hysteresis loops were recorded and presented in the Fig. 6. In the present case, undoped ZnO nanostructures show the paramagnetic behaviour and Er doped ZnO nanostructures expose the ferromagnetic hysteresis loop at room temperature. Since, there is no reason to attribute the introduction of ferromagnetism to any dopant and moreover in this ZnO case, there is no $3d$ electron involved, one cannot think of any interaction that may originate from that and hence, the undoped ZnO bulk is expected to diamagnetic in nature [50, 51]. Multiple nanostructures of either inorganic or organic systems have been reported to show magnetic properties in the absence of magnetic elements [52–56] and even the suggestion of magnetism as a universal feature at the nanoscale has been proposed [57].

This study focuses on the outcome of Er^{3+} ions on the magnetic behaviour of ZnO nanostructures at room temperature. Er is one of the RE elements, which has more than a half filled $4f$ electron shells ($4f^{11}6s^0$). We observe that, the saturation magnetization (M_S), remanent magnetization (M_R) and the coercivity (H_C) value increases from $x = 1$ at.% Er to $x = 7$ at.% Er doped ZnO nanostructures, and are listed in Table 2. As the Er concentration increases, all these parameters are in appropriate increasing order. The magnetic moment per Er ion, which was obtained from the M_S /total number of Er, decreased from $0.1439/\text{Er}$ ($x = 1$) to $0.5548/\text{Er}$ ($x = 5$). The origin of ferromagnetism in Er doped ZnO nanostructures might be caused by the exchange interactions between unpaired electrons spins arising from

Table 2 Values of saturation magnetization, remanent magnetization and coercivity of Er doped ZnO samples

Concentration of Er (%)	Saturation magnetization M_S (emu/g)	Remanent magnetization M_R (emu/g)	Coercivity H_C (Oe)
1	0.1439	0.0554	0.002
3	0.3691	0.1543	0.006
5	0.5548	0.1926	0.017
7	1.6297	0.3691	0.022

oxygen vacancies and/or defects and confinement effects at the surface of nanostructures [57]. Furthermore RE ions introduce spin polarized localized states in the band gap. The impurity states are determined by the interaction between dopant atomic states and the host lattice. The interaction of the atomic states with the VB or CB would form bonding and anti-bonding states. After bonding, every RE atom loses three electrons and becomes RE^{3+} i.e. Er^{3+} ion. On the other hand, the magnetic ion is characterized by localized $3d$ or $4f$ shells. The magnetic properties are decided by the localized magnetic moments associated with the magnetic ions and their interaction with the host semiconductor. The desired magnetic behaviour in the case of RE ions is s, p–f atoms. As we know, $4f$ RE atoms have larger magnetic moments compared to those of the $3d$ transition metal atoms [58, 59]. From this, it is clear that the magnetic moment was mainly contributed by the RE $4f$ orbital. Thus, Er doped ZnO nanostructures are observed to show dilute magnetic semiconducting behaviour.

4 Conclusion

In summary, undoped ZnO and a series of Er doped ZnO nanostructures samples were prepared by a chemical precipitation method and their structural, optical and magnetic properties as a function of doping concentration was undertaken. The foremost results from these studies are following: The XRD results showed that the undoped ZnO and Er doped ZnO nanostructures are single phase hexagonal ZnO and unwanted Er related compounds were not formed during the growth of Er doped ZnO nanostructures. EDX studies also showed that the Er ions were successfully integrated into the ZnO lattice sites. HRSEM images illustrated that the inclusion of Er ions in crystal structure of ZnO could significantly the morphological evolution of ZnO from nanorods-like to nanocones-like. These morphological changes could be explained by an increase of ZnO crystal growth rate along vertical direction due to doping of Er^{3+} ions in its crystal structure. Er dopant has a strong consequence on structural and optical properties, which could be shown in a considerable red shift in the band gap, the formation of new states

due to doping level and the presence of an oxygen vacancy. Values of optical band gap decrease from 3.34 to 3.19 eV for undoped ZnO nanostructures and 1–7 at.% Er doped ZnO nanostructures respectively. PL analysis revealed that the Er³⁺ ions doped ZnO has a high optical property and kind of fascinating PL material that shows multiemission peaks at the blue to yellowish-red region, which was attributed to the enhanced defects or oxygen vacancies in excess caused by Erbium oxide dopant. At room temperature the hysteresis was observed in the M–H curves shows the presence of ferromagnetism in all Er doped ZnO samples, and it is found that the coercivity, remanent magnetization and the saturation magnetization values of these samples increases as the doping concentration is gradually increased from 1 to 7 at.% Er. The results suggest the possibility that the introduction of Er into ZnO material prepared by chemical precipitation method have the potential to be used in photonic and spintronic device applications.

Acknowledgements The authors extend their gratitude to Dr. Anil Ahlawat (Offg. Director, KIET Group of Institutions, Ghaziabad) and Prof. C.M. Batra (Head, Department of Applied Sciences, KIET Group of Institutions, Ghaziabad) for their constant support and encouragement to carry out this work. The authors are thankful to Dr. Ashokan Kumar, Inter University Accelerator Centre, Delhi for VSM characterization.

References

- M. Timpel, M.V. Nardi, S. Krause, G. Ligorio, C. Christodoulou, L. Pasquali, A. Giglia, J. Frisch, B. Wegner, P. Moras, N. Koch, Surface modification of ZnO (0001)–Zn with phosphonate-based self-assembled monolayers: binding modes, orientation and work function. *Chem. Mater.* **26**, 5042–5050 (2014)
- M.H. Huang, S. Mao, H. Feick, H. Yan, Y. Wu, H. Kind, E. Weber, R. Russo, P. Yang, Room-temperature ultraviolet nanowire nanolasers. *Science* **292**, 1897–1899 (2001)
- D. Kim, K.Y. Lee, M.K. Gupta, S. Majumder, S.-W. Kim, Self-compensated insulating ZnO-based piezoelectric nanogenerators. *Adv. Funct. Mater.* **24**, 6949–6955 (2014)
- Y.-W. Wang, A. Cao, Y. Jiang, X. Zhang, J.-H. Liu, Y. Liu, H. Wang, Superior antibacterial activity of zinc oxide/graphene oxide composites originating from high zinc concentration localized around bacteria. *ACS Appl. Mater. Interfaces* **6**, 2791–2798 (2014)
- Y. Sun, J. Yang, L. Yang, M. Gao, X. Shan, Z. Zhang, M. Wei, Y. Liu, L. Fei, H. Song, Less contribution of nonradiative recombination in ZnO nanowires compared with rods. *J. Lumin.* **134**, 35–41 (2013)
- G. Zhu, Y. Zhou, S. Wang, R. Yang, Y. Ding, X. Wang, Y. Bando, Z. Wang, Synthesis of vertically aligned ultra-long ZnO nanowires on heterogeneous substrates with catalyst at the root. *Nanotechnology* **23**, 055604-1–055604-6 (2012)
- F.D. Nayeri, E.A. Soleimani, Influence of seed layers on the vertical growth of ZnO nanowires by low-temperature wet chemical bath deposition on ITO-coated glass substrate. *Exp. Tech.* **38**, 13–20 (2014)
- S. Anandan, A. Vinu, K.S. Lovely, N. Gokulakrishnan, P. Srinivasu, T. Mori, V. Murugesan, V. Sivamurugan, K. Ariga, Photocatalytic activity of La-doped ZnO for the degradation of monocrotophos in aqueous suspension. *J. Mol. Catal. A* **226**, 149–157 (2007)
- P.V. Kamat, Photochemistry on nonreactive and reactive (semiconductor) surfaces. *Chem. Rev.* **93**, 267–300 (1993)
- U. Ozgur, Y.I. Alivov, C. Liu, A. Teke, M.A. Reshchikov, S. Doğan, V. Avrutin, S.-J. Cho, H. Morkoc, A comprehensive review of ZnO materials and devices. *J. Appl. Phys.* **98**, 041301 (2005)
- N. Kilinc, S. Ozturk, L. Arda, A. Altindal, Z.Z. Ozturk, Structural, electrical transport and NO₂ sensing properties of Y-doped ZnO thin films. *J. Alloys Compd.* **536**, 138–144 (2012)
- Z.K. Heiba, L. Arda, M.B. Mohamed, Structural and magnetic properties of Zn_{0.95}Cr_{0.05}O annealed at different temperatures. *J. Magn. Magn. Mater.* **389**, 153–156 (2015)
- N. Kilinc, L. Arda, S. Ozturk, Z.Z. Ozturk, Structure and electrical properties of Mg-doped ZnO nanoparticles. *Cryst. Res. Technol.* **45**, 529–538 (2010)
- Z.K. Heiba, L. Arda, Structural properties of Zn_{1-x}Mg_xO nanomaterials prepared by sol–gel method. *Cryst. Res. Technol.* **44**, 845–850 (2009)
- S. Gburt, D. Stichtenoth, S. Muller, W. Dewald, C. Ronning, J. Wang, Y. Jiao, Y.Y. Rao, S.K. Hark, Q. Li, Rare earth doped zinc oxide nanowires. *Nanosci. Nanotechnol.* **8**, 244–251 (2008)
- Y.R. Jang, K.H. Yoo, J.S. Ahn, C. Kim, S.M. Park, 1.54 μm emission mechanism of Er-doped zinc oxide thin films. *Appl. Surf. Sci.* **257**, 2822–2824 (2011)
- R. Vettumpperumal, S. Kalyanaraman, R. Thangavel, Optical constants and near infrared emission of Er doped ZnO sol–gel thin films. *J. Lumin.* **158**, 493–500 (2015)
- J.H. Shim, T. Hwang, S. Lee, J.H. Park, S.J. Han, Y.H. Jeong, *Appl. Phys. Lett.* **86**, 082503 (2005)
- B. Khalil, S. Naji, H. Labrim, M. Bhihi, A.G.E.L. Hachimi, M. Lakhal, A. Belhaj, A. Benyoussef, A. El Kenz, Magnetic properties of SrO doped with 3d transition metals. *J. Supercond. Nov. Magn.* **27**, 203–208 (2014)
- X. Ma, The magnetic properties of Gd doped ZnO nanowires. *Thin Solid Films* **520**, 5752–5755 (2012)
- Y. Tan, Z. Fang, W. Chen, P. He, Structural, optical and magnetic properties of Eu-doped ZnO films. *J. Alloys Compd.* **509**, 6321–6324 (2011)
- D.K. Sharma, K.K. Sharma, V. Kumar, A. Sharma, Effect of Ce doping on the structural, optical and magnetic properties of ZnO nanoparticles. *J. Mater. Sci.* **27**, 10330–10335 (2016)
- T. Schmidt, G. Muller, L. Spanhel, K. Kerkel, A. Forchel, Activation of 1.54 μm Er³⁺ fluorescence in concentrated II–VI semiconductor cluster environments. *Chem. Mater.* **10**, 65–71 (1998)
- D. Rute, W. Bauhofe, Highly luminescent Eu³⁺ or Tb³⁺ doped and ZnO sensitized optical fibers drawn from silicon compatible sealing glasses. *Appl. Phys. Lett.* **69**, 892 (1996)
- B. Yan, X. Chen, J. Wu, Induced assembly and photoluminescence of lanthanum (Tb, Eu, Dy) complexes/ZnO/polyethylene glycol hybrid phosphors. *Appl. Surf. Sci.* **253**, 8575–8580 (2007)
- R. Rolli, K. Gatterer, M. Wachtler, M. Beettinelli, A. Speghini, D. Ajo, Optical spectroscopy of lanthanide ions in ZnO–TeO₂ glasses. *Spectrochim. Acta Part A* **57**, 2009–2017 (2001)
- M. Kohls, T. Schmidt, H. Katschorek, L. Spanhel, G. Muller, N. Mais, A. Wolf, A. Forchel, A simple colloidal route to planar micropatterned Er@ZnO amplifiers. *Adv. Mater.* **11**, 288–292 (1999)
- H.L. Han, L.W. Yang, Y.X. Liu, Y.Y. Zhang, Q.B. Yang, Up-conversion luminescence switching in Er³⁺-containing ZnO nanoparticles through Li⁺ co-doping. *Opt. Mater.* **31**, 338–341 (2008)
- Y. Sun, Y. Chen, L. Tian, Y. Yu, X. Kong, Q. Zeng, Y. Zhang, H. Zhang, Morphology-dependent upconversion luminescence of ZnO:Er³⁺ nanocrystals. *J. Lumin.* **128**, 15–21 (2008)

30. Y.K. Ryu, P. Fernández, J. Piqueras, Growth and characterization of Er-doped ZnO elongated nanostructures. *Phys. Status Solidi A* **208**, 868–873 (2011)
31. Y.H. Yang, Y. Feng, H.G. Zhu, G.W. Yang, Growth, structure, and cathode luminescence of Eu-doped ZnO nanowires prepared by high-temperature and high-pressure pulsed-laser deposition. *J. Appl. Phys.* **107**, 053502 (2010)
32. Y. Terai, K. Yoshida, M.H. Kamarudin, Y. Fujiwara, Photoluminescence properties of Eu^{3+} ions in Eu-doped ZnO grown by sputtering-assisted metal organic chemical vapor deposition. *Phys. Status Solidi C* **8**, 519–521 (2010)
33. S.L. Romero, M.J.Q. Jiménez, M.H. García, A.A. Castillo, Bright red luminescence and structural properties of Eu^{3+} ion doped ZnO by solution combustion technique. *World J. Condens. Matter Phys.* **4**, 227–234 (2014)
34. E. Asikuzun, O. Ozturk, L. Arda, A.T. Tasci, F. Kartal, C. Terzioğlu, High-quality c-axis oriented non-vacuum Er doped ZnO thin films. *Ceram. Int.* **42**, 8085–8091 (2016)
35. R. John, R. Rajakumari, Synthesis and characterization of rare earth ion doped nano ZnO. *Nano-Micro Lett.* **4**, 65–72 (2012)
36. N.K. Divya, P.P. Pradyumn, Solid state synthesis of erbium doped ZnO with excellent photocatalytic activity and enhanced visible light emission. *Mater. Sci. Semicond. Process.* **41**, 428–435 (2016)
37. R. Zamiri, A.F. Lemos, A. Reblo, H.A. Ahangar, J.M.F. Ferreira, Effects of rare-earth (Er, La and Yb) doping on morphology and structure properties of ZnO nanostructures prepared by wet chemical method. *Ceram. Int.* **40**, 523–529 (2014)
38. X.Y. Kong, Z.L. Wang, Polar-surface dominated ZnO nanobelts and the electrostatic energy induced nanohelices, nanosprings, and nanospirals. *Appl. Phys. Lett.* **84**, 975 (2004)
39. L. Yang, Z. Wang, Z. Zhang, Y. Sun, M. Gao, J. Yang, Y. Yan, Surface effects on the optical and photocatalytic properties of graphene like ZnO:Eu³⁺ nanosheets. *J. Appl. Phys.* **113**, 033514 (2013)
40. F. Li, X.-C. Liu, R.-W. Zhou, H.-M. Chen, S.-Y. Zhuo, E.-W. Shi, Strong correlation between oxygen vacancy and ferromagnetism in Yb-doped ZnO thin films. *J. Appl. Phys.* **116**, 243910 (2014)
41. S. Chauhan, M. Kumar, S. Chhoker, S.C. Katyal, V.P.S. Awana, Structural, vibrational, optical and magnetic properties of sol–gel derived Nd doped ZnO nanoparticles. *J. Mater. Sci.* **24**, 5102–5110 (2013)
42. M. Kachi, W. Sakamoto, M. Ichida, T. Wada, H. Ando, T. Yogo, Synthesis of Er-doped ZnO nanoparticle/organic hybrid from metal-organics. *J. Mater. Sci.* **47**, 5128–5133 (2012)
43. L. Irimpan, V.P.N. Nampoore, P. Radhakrishnan, A. Deepthy, B. Krishnan, Size dependent fluorescence spectroscopy of nanocolloids of ZnO. *J. Appl. Phys.* **102**, 063524 (2007)
44. R.M. Nyffenegger, B. Craft, M. Shaaban, S. Gorer, G. Erley, R.M. Penner, A hybrid electrochemical/chemical synthesis of zinc oxide nanoparticles and optically intrinsic thin films. *Chem. Mater.* **10**, 1120–1129 (1998)
45. A. Mohanta, R.K. Thareja, Photoluminescence study of ZnO nanowires grown by thermal evaporation on pulsed laser deposited ZnO buffer layer. *J. Appl. Phys.* **104**, 044906 (2008)
46. O. Madelung, *Semiconductors: Data Handbook*, 3rd edn., (Springer, Berlin, 2003)
47. L.V. Azaroff, *Introduction to Solids* (McGraw-Hill, New York, 1960), pp. 371–372
48. P. Schröer, P. Krüger, J. Pollmann, First-principles calculation of the electronic structure of the wurtzite semiconductors ZnO and ZnS. *Phys. Rev. B* **47**, 6971 (1993)
49. V. Kumar, H.C. Swart, O.M. Ntwaeaborwa, R.E. Kroon, J.J. Terblans, S.K.K. Shaat, A. Yousif, M.M. Duvenhage, Origin of the red emission in zinc oxide nanophosphors. *Mater. Lett.* **101**, 57–60 (2013)
50. S. Zhou, K. Potzger, H. Reuther, K. Kuepper, W. Skorupa, M. Helm, J. Fassbender, Absence of ferromagnetism in V-implanted ZnO single crystals. *J. Appl. Phys.* **101**, 09H109 (2007)
51. N.H. Hong, J. Sakai, V. Brizé, Observation of ferromagnetism at room temperature in ZnO thin films. *J. Phys.* **19**, 036219 (2007)
52. R. Nascimento, A.J.A. de Oliveira, A.A. Correa, L.O. Bulhoes, E.C. Pereira, V.M. Souza, L. Walmsley, Magnetic behavior of poly(3-methylthiophene): metamagnetism and room-temperature weak ferromagnetism. *Phys. Rev. B* **67**, 144422 (2003)
53. F.R. de Paula, L. Walmsley, E.C. Pereira, A.J.A. Oliveira, Magnetic properties of poly(3-hexylthiophene). *J. Magn. Mater.* **320**, e193–e195 (2008)
54. D. Gao, Z. Zhang, J. Fu, Y. Xu, J. Qi, D. Xue, Room temperature ferromagnetism of pure ZnO nanoparticles. *J. Appl. Phys.* **105**, 113928 (2009)
55. S. Deng, K.P. Loh, J.B. Yi, J. Ding, H.R. Tan, M. Lin, Y.L. Foo, M. Zheng, C.H. Sow, Room temperature ferromagnetism at self-assembled monolayer modified Ag nanocluster–ZnO nanowire interface. *Appl. Phys. Lett.* **93**, 193111 (2009)
56. O.V. Yazyev, Emergence of magnetism in graphene materials and nanostructures. *Rep. Prog. Phys.* **73**, 056501 (2010)
57. A. Sundaresan, C.N. Rao, Implications and consequences of ferromagnetism universally exhibited by inorganic nanoparticles. *Solid State Commun.* **149**, 1197–1200 (2009)
58. A.G. El Hachimi, H. Zaari, A. Benyoussef, M. El Yadari, A. El Kenz, First-principles prediction of the magnetism of 4f rare-earth-metal-doped wurtzite zinc oxide. *J. Rare Earths* **32**, 715–721 (2014)
59. J. Xie, First-principles study on the magnetism in ZnS-based diluted magnetic semiconductors. *J. Magn. Mater.* **322**, L37–L41 (2010)